DC-to-DC Converter with Low Input Current Ripple for Maximum Photovoltaic Power Extraction

Abstract—This paper presents a dc-to-dc converter, which offers continuous input and output energy flow, and low input current ripple, applicable and mandatory for photovoltaic arrays, and maximum power point tracking applications. The PV array yields exponential curves for current and voltage where the maximum power occurs at the curve's mutual knee. Conventional dc-to-dc converters have a relatively high input ripple current which causes high power losses when connected to nonlinear sources like PV arrays. The proposed converter operates with low input current ripple which maximizes the power that can be sourced from the PV array, without the need of any electrolytic filtering capacitance. The effect of the ripple current on the PV array can be significant, and decreases the efficiency of the PV system. The proposed converter employs series input inductance with both input and output continuous energy flow. Converter simulations and experimental results support and extol the system concept.

Index terms—Constant current converters, dc-to-dc converters, dc-to-dc power conversion, photovoltaic cells, and switched-mode power supplies.

I. INTRODUCTION

OWING to the need for maximum utilization of solar cells, fuel cells, wind turbines, and batteries, dc-to-dc converters with continuous input energy flow are widely used for renewable energy applications [1]-[3]. To save energy, rather than converting to another energy form, the photovoltaic (PV) source output current and voltage should be continuous (and non-zero) for maximum renewable energy extraction. Also the dc-to-dc converters must assure continuous input and output current to provide maximum energy flow from the source to the load. Therefore, an *LC* filter, a large capacitor, or a continuous current converter can be adopted for continuous PV output energy. Adding either an *LC* or a *C* filter can create electrical resonance issues, costs money, increases weight and volume, plus decreases reliability, particularly in the case of electrolytic capacitors. In avoiding these issues, the PV must draw continuous current to provide better maximum power point tracking (MPPT) with minimal energy ripple [4].

Power supplies employ electrolytic capacitors for energy storage and to reduce input current and output voltage ripple. Although electrolytic capacitance can be large, such capacitors have a short lifetime owing to the liquid electrolyte, thus restricting performance enhancement of the long lifetime system [5]-[7]. The lifetime of the electrolytic capacitor is limited to a few thousand hours at rated operating conditions [5], which is shorter than the lifetime of other components like light emitting diodes (LEDs), lead-acid batteries, and photovoltaic panels. Thus, the electrolytic capacitor is an obstacle to the overall reliability of photovoltaic converter systems, thus is significantly derated. The lifetime may only be 1000 hours at rated conditions, while every 10°C operating temperature decrease, doubles the lifetime. The LEDs lifetime is generally higher than 80 thousand hours [8], while the lead-acid batteries life-time reaches ten years and additionally is recyclable [9].

The current ripple creates a problem in power electronic systems, which affects the voltage and, thus, the power. The extent of the loss problem due to PV current ripple is a feature realized for the first time in this paper. The PV cell yields exponential curves for current and voltage, where the maximum power occurs at the curve's mutual knee. This exponential curve causes nonlinear mapping in the current axis which in turns leads to high loss of output power due to the input ripple current. With current ripple the controller, which will have a bandwidth less than the converter switching frequency, does not operate around the dc MPP. Rather the average point is changed when extracting maximum power. As the ripple current decreases the average operating point converges to the dc operating MPP. The assessment of converter interfacing for photovoltaic sources has underlying decoupling capacitance requirements to operate at maximum power with minimal ripple [10]-[14], with large capacitance filtering needed for converters with discontinuous input current.

The actual power losses are considerably larger expected by modest small-signal approaches. The higher drop in power is clarified in [10], studied in [15]-[18], and experimentally established in [15], [17] and [18]. In [15], the authors establish that 8% ripple rms amplitude of the MPP voltage results in 5% drop in photovoltaic power output which is the 5% of the PV efficiency. Under non-uniform irradiance, this percentage loss can be significantly higher and such results are confirmed in this paper. In [10] and [16], the authors considered sensitivity to ripple in voltage and current at the terminals of the PV module. Their simulations verify a power loss of 1% when the amplitude of the ripple voltage is equal to 6% of the MPP voltage, and a loss of 2% for an 8.5% voltage ripple. Such effects have not been studied extensively in the literature, particularly the effects of the current ripple (as opposed to voltage ripple) on the PV module; in terms of MPPT design or ripple from the DC-to-DC converter. In [15], the losses reaches 5%, while in [16] losses reach 2% of the PV efficiency at around 8% ripple of the MPP voltage. This because many factors affect the percentage loss, such as, irradiance level, fill factor of the PV module and non-uniform weather conditions. In this paper, as established in the previous studies, the higher the irradiance level, the lower the effect of the ripple current, yet, the lower the irradiance level, the greater the effect of the ripple current, hence, the lower the PV efficiency.

The criteria for PV dc-to-dc converter [19]-[22] selection depend on many factors such as cost, efficiency, flexibility, and energy flow. Flexibility here represents the ability of the converter to maintain the output with the input varying, while energy flow is assured by the continuous input and output current of the converter. This paper classifies converter based on flexibility, energy flow, and number of components, hence 'cost'. Among known converters, the SEPIC, buck-boost, and Ćuk converters have the ability to step up and step down the input voltage, hence can transfer energy for all irradiation levels. Another desirable feature is continuous output current, which allows converter output parallel connection, or conversion to a voltage source with minimal shunt capacitance. The buck or boost converters are not preferable due to the lack of output voltage magnitude flexibility. Both buck and buck-boost converters have discontinuous input current, while the SEPIC converter has discontinuous output current with more components. The only commonly used converter that achieves continuous input and output current, flexible output (step up/down

voltage), and a low number of components (two inductors, one capacitor, one switch, and one diode) is Ćuk converter.

The flexible buck-boost transfer function of the Ćuk converter can be implemented by reconfiguring the same components to create a further two different converters, all with continuous input and output current, as shown in Fig. 1. The Ćuk converter is shown in Fig. 1a. In this paper the second converter (Fig. 1b) is called the 'C converter', and the third converter (Fig. 1c) is called the 'D converter'.
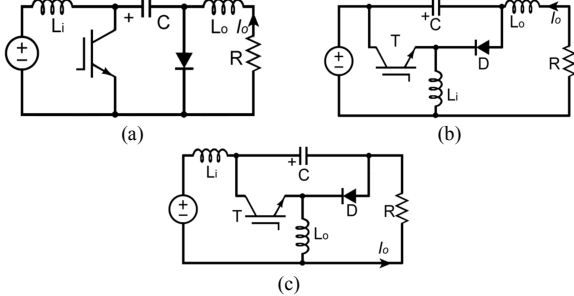

Fig. 1: Converters with buck-boost transfer function, continuous input/output current, and same number of components: (a) Ćuk, (b) C, and (c) D.

This paper considers three converters, and proposes converter D as an effective solution to input ripple current reduction for the PV source achieving the maximum overall efficiency. As well as continuous input and output current for continuous energy flow, it produces near zero input ripple current (without inductor coupling), which affects the PV array when tracking maximum power around the PV *I-V* knee. The low input current ripple affects significantly the PV efficiency, which is the factor that mitigates the lower efficiency of the D converter, to produce the highest overall system efficiency over the three converters, when using the same converter components.

II. THE EFFECT OF INPUT RIPPLE CURRENT

Ripple current refers to small variations of the dc signal encountered in power supply applications. Input ripple current from a switching power supply contains harmonics, necessitating proper design to reduce the ripple. To achieve low-ripple current, filtering approaches are commonly used, which usually utilize large reactive components to assure effective suppression of significant low-order harmonic components. The use of large filters, however, is not an economical solution for switching power supplies.

The concept of power supply zero-ripple input current is not new. It is used to increase the power density of the converter, therefore is of considerable interest in switching converters. Two reasons at least make it necessary to reduce the input ripple current. First, it reduces the stress on the capacitors, resulting in either lower power losses or relaxed filter stresses. Second, it decreases the noise conducted to the load, where most converters have a pulsating current at either the input or output [23]-[24].

In addition to the mentioned effects of the input ripple current in conventional power supplies, ripple has a significant effect when associated with a PV module. As shown in Fig. 2, an ideal voltage source does not reflect any ripple and this also occurs for voltage ripple in the ideal current source case. Normally, current and voltage sources are not ideal and the input resistance reflects small ripple on both the voltage/current curves when the input current/voltage has ripple. The PV source can operate as either a voltage or current source, and can also be considered as both a current and voltage source. The PV module is a dynamic energy source that has dc output voltage and

current. Fig. 3 sheds light on the effect of the ripple current on the power curve, where due to the curve knee, significant output power is lost as the current (hence power) ripple increases. Unfortunately, the PV source characteristics change due to the weather conditions; temperature and radiation, which increase the losses. Maximum power tracking algorithms based on maximum average power are not MPP trackers. As ripple current increases the operating point moves towards the constant voltage region of the PV characteristic, which results in a sharp decline in the average power. By maximizing the average power, the mean operating point moves toward the MPP as the ripple current reduces to zero.

By achieving maximum power using any MPPT algorithm, maximum dc power cannot be achieved if current ripple exist. For zero-ripple input current, the maximum power can be achieved since the PV cell MPP can be tracked.

An exponential diode model of solar panel with same cells, irradiation, and temperature is used to calculate the expression for the ripple current in (1).
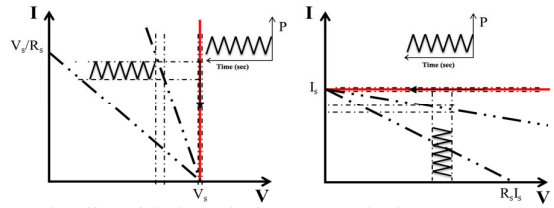

Fig. 2: The effect of the input ripple current on the dc power supply.

$$i(t) = I_{sc} - I_s \left(e^{\frac{v(t)}{mV_T}} - 1 \right) \tag{1}$$

Similarly

$$v(t) = mV_T \ln \left(\frac{I_{sc} - i(t)}{I_s} + 1 \right) \tag{2}$$

where $v(t)$ is the panel voltage, $i(t)$ is the panel current, I_{sc} is the short-circuit current, m is the number of cells, V_T is thermal voltage, and I_s is scale current.
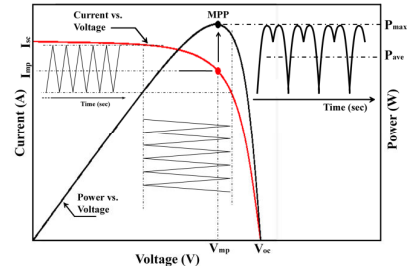

Fig. 3: The effect of input ripple current on the PV power curve.

The output power of the PV panel is the product of voltage and current, and can be transcribed in terms of $i(t)$

$$P(t) = i(t)mV_T \ln \left(\frac{I_{sc} - i(t)}{I_s} + 1 \right) \tag{3}$$

Using Taylor series expansion of $P(v(t))$, the power of any operating point, (V_x, I_x), can be approximated as follows:

$$p(t) = V_x I_x + \Delta i(t) \frac{dP}{di} + \frac{1}{2} \Delta i(t)^2 \frac{d^2 P}{di^2} \tag{4}$$

at MPP, (V_{mpp}, I_{mpp}), the first derivative is zero; $dP/di = 0$. Then, the power at MPP can be expressed as in (5):

$$p(t) = V_{mpp} I_{mpp} + \frac{1}{2} \Delta i(t)^2 \frac{d^2 P}{di^2} \tag{5}$$

The mean reduction in power collected can be expressed in terms of the rms value of rippled voltage, $(\Delta i)_{rms}$, as shown in (6)

$$P_{ripple} = -\frac{1}{2}(\Delta i_{rms})^2 \frac{d^2P}{di^2} \qquad (6)$$

The first derivative at the MPP is zero, while the first derivative can be derived as follow:

$$\frac{dP}{di} = i\frac{dv}{di} - v \qquad (7)$$

at MPP:

$$\frac{dv}{di} = \frac{V_{mpp}}{I_{mpp}} = R_{ss} \qquad (8)$$

where R_{ss} is the small signal resistance at the MPP. The first and second derivative of P in terms of i can be derived from (3) as shown in (9) and (10) respectively:

$$\frac{dP}{di} = mV_T i(t)\left(\frac{-1}{I_s + I_{sc} - i(t)}\right) + mV_T \ln\left(\frac{I_s + I_{sc} - i(t)}{I_s}\right) \quad (9)$$

$$\frac{d^2P}{di^2} = \left(\frac{-2mV_T}{I_s + I_{sc} - i(t)}\right) - \left(\frac{mV_T i(t)}{(i(t) - I_s - I_{sc})^2}\right) \qquad (10)$$

at MPP:

$$V_{mpp} = \left(\frac{mV_T I_{mpp}}{I_s + I_{sc} - I_{mpp}}\right) = mV_T \ln\left(\frac{I_s + I_{sc} - I_{mpp}}{I_s}\right) \qquad (11)$$

where,

$$\frac{V_{mpp}}{I_{mpp}} = \frac{mV_T}{I_s + I_{sc} - I_{mpp}} \qquad (12)$$

$$R_{ss} = \frac{mV_T}{I_s + I_{sc} - I_{mpp}} \qquad (13)$$

By substituting (13) in (10), the second derivative can be as follows:

$$\frac{d^2P}{di^2} = -2R_{ss} - \frac{R_{ss}^2 I_{mpp}}{mV_T} \qquad (14)$$

By substituting (14) in (6), the input current ripple can be as follows:

$$P_{ripple} = (\Delta i_{rms})^2 \left[R_{ss} + \frac{R_{ss}^2 I_{mpp}}{2mV_T}\right] \qquad (15)$$

The rippled power can be expressed as a fraction of MPP power in terms of the current ripple as follows:

$$\frac{P_{ripple}}{P_{mpp}} = \left(\frac{\Delta i_{rms}}{I_{mpp}}\right)^2 \left[1 + \frac{V_{mpp}}{2mV_T}\right] \qquad (16)$$

for typical values $V_{mpp} = 0.5V$ per cell, and $V_T = 25.85mV$, (16) can be written as follows:

$$\frac{P_{ripple}}{P_{mpp}} = 10.67\left(\frac{\Delta i_{rms}}{I_{mpp}}\right)^2 \qquad (17)$$

Current ripple with an rms value equal to *5%* of the MPP current would result in a *2.7%* reduction in power output and current ripple with *8%* would result in power output reduction of *6.83%*, which is big enough to reduce the overall efficiency of an effective converter.

Moreover, efficiency loss depends on the control method used for the converter. The converter can be controlled in open or closed loop. For an open loop switched converter, the output power depends on the average rippled input current, while for the closed loop switched converter system, the output power is the average rippled output power. For an open loop converter, the MPPT may operate on the average MPPT current, which is the same PV MPP without current ripple. In this case, the power curve has consecutive small and large power dips, as shown in Fig. 4, which causes loss

of converter input power. Fig. 4 presents the power curves at different input ripple current percentages (10% to 95% of the short circuit current), giving the average power and efficiencies in Table I, at 1000W/m² and 25°C for a specific PV module. For a closed loop controlled converter, the controller will move the average operating point more towards the voltage limit, so that the small dip increases, while the large dip decreases. Thus, the 'average' MPP is different to the point without ripple because the ripple deviates the MPP depending on the average rippled PV power. Similarly, Fig. 5 presents the power curves of the closed loop converter at different ripple current percentages, with the average power and efficiencies in Table I, at 1000W/m² and 25°C. The PV power can drop by up to 30% the available power before considering the converter efficiency. Figs. 4 and 5 only focus on the effect of the input ripple current on the PV curve, before considering converter losses. The overall efficiency is a combination of both the PV efficiency and the converter efficiency, which must be considered to determine the most effective converter. Large current ripple is not a desirable condition in a dc-to-dc converter because worst cases, the input current ripple should not reach 50% of the short circuit current. However, the high ripple extremes in Figs. 4 and 5 are shown to accentuate and generalize the problem under wide input current ripple conditions.

TABLE I
THE RELATION BETWEEN INPUT RIPPLE CURRENT
AND THE PV EFFICIENCY FOR (A) OPEN LOOP
CONVERTER, AND (B) CLOSED LOOP CONVERTER.

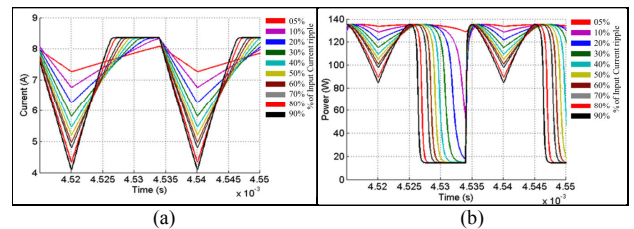| (a)			(b)		
Open loop			Closed loop		
% I_{sc}	P_{ave}	PV η%	% I_{sc}	P_{ave}	PV η %
05	133.3	98.0	05	132.3	97.3
10	127.7	93.9	10	129.9	95.5
20	118.1	86.8	20	127.6	93.8
30	109.5	80.5	30	122.2	89.8
40	102.8	75.6	40	116.2	85.5
50	97.6	71.8	50	110.3	81.1
60	92.8	68.3	60	103.3	76.0
70	89.1	65.4	70	96.7	71.1
80	81.9	60.2	80	74.7	54.9
90	77.6	57.1	90	41.4	30.4

(a)   (b)
Fig. 4:(a) Input ripple current, (b) PV power, for open loop system.
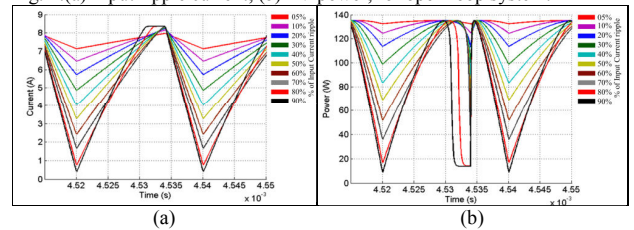

(a)   (b)
Fig. 5: (a) Input ripple current, (b) PV power, for closed loop system.

The effects of the input ripple current increases by decreasing the peak of the PV power curve. This is because the current ripple depends on the converter while the knee (which causes the losses) of the power curve depends on the radiation. Thus, by either decreasing the irradiation or

operating with small current, the percentage of the ripple current as well as the losses increase.

In Table I, the open loop efficiency is high for small ripple but rapidly decreases for higher ripple, while the closed loop efficiency starts lower than that of the open loop case, but is higher than that of open loop case for higher ripple.

III. INPUT AND OUTPUT POWER

The feature of the continuous input and output power of a dc-to-dc converter guarantees the effectiveness of a converter. The input and output current can be either continuous or discrete, with or without ripple, giving either continuous or discrete energy flow hence affecting the input source efficiency or the output load application.

A load shunt capacitor converts a current source to a voltage source. Both the Ćuk converter and the C converter use output series inductance to provide a current source. The series inductance provides an ac-free, dc component of the load signal. A load shunt capacitor bypasses the ac current components, while the dc output current component flows through the load. Similarly, series input inductance converts a constant current source to a constant voltage source. Passive components like capacitors and inductors can be used to temporarily store energy in the case of the discontinuity or short circuiting of a current source. Although large inductance provides a robust continuous current source, the transient response is slow, while losses and cost increase. The converters that have physical input inductance are the Ćuk and D converters thus these can operate as a continuous input current source [4]. Thus the Ćuk converter can have continuous input and output current, the C converter can be a continuous output current source, and the D converter can be a continuous input current source.

The general structure of a dc-to-dc converter is presumed as shown in Fig. 6, where the converter consists of three main parts: the input source, the converter topology, and the output port. The converter topology is defined as a combination of capacitors, inductors, and switches arranged such that when the input source and the output port are appropriately connected, the duty cycle controls the transfer function between input and output, hence the output port can deliver power. With this arrangement, the converter topology has three terminals.

In Fig. 6, by Kirchhoff's current law, the three terminal current components must be zero, that is $I_{T1}+I_{T2}+I_{T3}=0$. Consequently, in steady-state, the current must be continuous or continuously zero at one terminal if the other two terminals draw continuous current. As a result, both the C and D converters, despite only having either input or output inductance, can have continuous current at all terminals. Both the C and D converters have inductance at terminal T_3 that is effectively superimposed to give continuity of either the input or output current, respectively.

Thus the three converters shown in Fig. 1 all have continuous input and continuous output currents, with a switch, diode, two inductors, and one capacitor. Moreover, each has a step-up/step-down (flexible) transfer function.
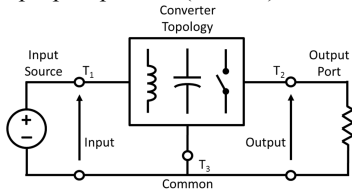

Fig. 6: General structure of dc-to-dc converters.

IV. ANALYSIS OF THE D CONVERTER

This simplified representation of D converter in Fig. 7 permits derivation of a dynamic model. The D converter has two modes of operation. The first is when the transistor is ON and, the diode is reverse biased, creating an open circuit. Simultaneously, L_1 and L_2 draw current from the voltage source. This is the energizing mode. The second mode starts when the transistor is turned OFF and the diode becomes forward biased, creating a short circuit. This is the discharging mode because the energy stored in the inductor L_1 is transferred to the load.

As mentioned in the introduction, the D converter has a specific feature which is low input ripple current that will be verified later in this section. When the switch is on, the two inductors are effectively series connected across the source, so the input ripple current is controlled by the two inductors.

To obtain the transfer function describing the D converter, the ideal topology is considered in Fig. 7. The equations describing the converter are derived by using Kirchhoff's current and voltage laws. D converter operation starts when the switch turns on at time $t=0$, and the current in inductor L_1 increases and the voltage on the capacitor turns off the diode. Capacitor C_1 discharges energy to the circuit when the switch turns off at time $t=t_x$. Fig. 7 shows the diode and the switch providing synchronous switching action.
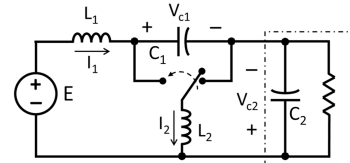

Fig. 7: D converter circuit showing synchronization of switch and diode.

A magnified viewed of the current through L_1 is as shown in Fig. 8, where the current I_1 is assumed linearly during the period t_{on}. From Fig. 8, equation (18) can be derived:

$$E = L_1 \frac{I_{tx} - I_{t0}}{t_{on}} + L_2 \frac{I_{tZ} - I_{tY}}{t_{on}} = L_1 \frac{\Delta I_1}{t_{on}} + L_2 \frac{\Delta I_2}{t_{on}} \quad (18)$$

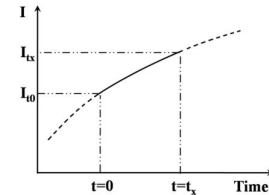$$t_{on} = \frac{\Delta I_1 L_1 + \Delta I_2 L_2}{E} \quad (19)$$

Fig. 8: View of the current through inductor L_1.

I_{t0} is the starting current at time $t=0$, I_{tx} is the current at time $t=t_x$ in the inductor L_1, I_{tZ} is the starting current, I_{tY} is the current at time $t=t_{on}$ in the inductor L_2, t_{on} is the switch ON time, and t_{off} is the switch OFF time, assuming continuous conduction.

During the charging of C_1, L_1 current falls linearly.

$$E - V_{c1} = -\left(L_1 \frac{\Delta I_1}{t_{off}} + L_2 \frac{\Delta I_2}{t_{off}} \right) \quad (20)$$

$$t_{off} = \frac{-\Delta I_1 L_1 - \Delta I_2 L_2}{E - V_{c1}} \quad (21)$$

The switch on-state duty cycle δ, for a cycle period T, is:

$$t_{on} = \delta T \quad (22)$$

$$t_{off} = (1 - \delta)T \quad (23)$$

Substituting (22) and (23) into (19) and (21) respectively gives

$$V_{c1} = \frac{E}{1-\delta} \qquad (24)$$

Assuming the current in L_2 rises linearly from I_{tY} to I_{tZ} in time t_{on}, then:

$$V_{c1} - V_{c2} = L_2 \frac{I_{tZ} - I_{tY}}{t_{on}} = \frac{L_2 \Delta I_2}{t_{on}} \qquad (25)$$

whence

$$t_{on} = \frac{L_2 \Delta I_2}{V_{c1} - V_{c2}} \qquad (26)$$

The current falls linearly from I_{tZ} to I_{tY} in time t_{off}, so:

$$V_{c2} = L_2 \frac{\Delta I_2}{t_{off}} \qquad (27)$$

where

$$\Delta I_2 = I_{tZ} - I_{tY} \qquad (28)$$

$$t_{off} = \frac{L_2 \Delta I_2}{V_{c2}} \qquad (29)$$

From (25) and (27):

$$\Delta I_2 = \frac{t_{on}(V_{c1} - V_{c2})}{L_2} = \frac{t_{off} V_{c2}}{L_2} \qquad (30)$$

$$V_{c1} = \frac{V_{c2}}{\delta} \qquad (31)$$

From (24) and (31):

$$\frac{V_{c2}}{E} = \frac{\delta}{1-\delta} = H(\delta) \qquad (32)$$

The switching period T can be found from equations (19) and (21):

$$T = \frac{1}{f} = t_{on} + t_{off} = \frac{\Delta I_1 L_1 + \Delta I_2 L_2}{E} + \frac{-\Delta I_1 L_1 - \Delta I_2 L_2}{E - V_{c1}}$$
$$= \frac{-(\Delta I_1 L_1 + \Delta I_2 L_2) V_{c1}}{E(E - V_{c1})} \qquad (33)$$

From equations (26) and (29):

$$T = \frac{1}{f} = t_{on} + t_{off} = \frac{L_2 \Delta I_2}{V_{c1} - V_{c2}} + \frac{L_2 \Delta I_2}{V_{c2}} = \frac{\Delta I_2 L_2 V_{c1}}{(V_{c1} - V_{c2}) V_{c2}} \qquad (34)$$

It can be concluded from (34) that the ripple current in inductor L_2 is:

$$\Delta I_2 = \frac{(V_{c1} - V_{c2}) V_{c2}}{L_2 V_{c1} f} \qquad (35)$$

The input ripple current in inductor L_1 can be found by substituting (35) into (33):

$$\Delta I_1 = \frac{-(V_{c1} - V_{c2}) V_{c2} - E(E - V_{c1})}{V_{c1} L_1 f} \qquad (36)$$

Equation (36) is an important conclusion from this analysis: it is the input ripple current for the D converter.
By substituting (24) and (31) into (36), gives the input ripple current in terms of the charging capacitor voltage:

$$\Delta I_1 = \frac{-(1-\delta)\delta V_{c1} + (1-\delta)\delta V_{c1}}{L_1 f} \qquad (37)$$

Similarly, the ripple input current is zero which is surprising conclusion for this converter. Equation (37) can be simply written as in (38):

$$\Delta I_1 = 0 \qquad (38)$$

In equation (38), the input ripple current for the D converter becomes zero compared with other converters like the Ćuk converter. By applying the same analysis to the Ćuk converter, the input ripple current for the Ćuk converter can be drawn in equation (39)

$$\Delta I_1 = \frac{V_{c1}(1-\delta)\delta}{L_1 f} \qquad (39)$$

The input current ripple can be zero if equation (40) is applied.

$$V_{c1}(1-\delta) = 0 \qquad (40)$$

That is, the input ripple current is zero only if either the duty cycle is one or the capacitor voltage is zero, which is impossible without switching off the power. This small ripple current gives leads to system efficiency maximization, as considered in the next two sections and confirmed by simulation and experimental results. The ripple reduction effect outweighs the better efficiency of the Ćuk converter. The reduced efficiency of converters C and D is primarily due to the fact that inductor L_2 conducts the sum of the input and output current, hence has higher copper $I^2 R$ losses.

Summarizing, Fig. 9 presents the input current ripple versus duty cycle, theoretically from equations (20) and (22) for different values of switching frequency (from 10kHz to 50kHz). Theoretically, the D converter shows significant reduction in input current ripple, much less than the Ćuk converter.
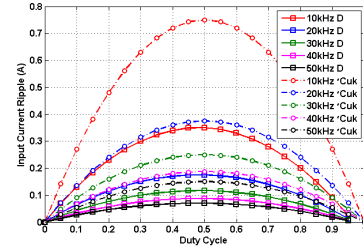

Fig. 9: Theoretical, input current ripple versus duty cycle for Ćuk and D converters at switching frequencies from 10kHz to 50kHz.

V. SIMULATION AND PRACTICAL RESULTS

MATLAB simulations are used to verify the performance of the three converters; Ćuk, C, and D converters. The simulations are at a 50kHz converter switching frequency, with a *Kyocera KD135GX-LP* photovoltaic module (V_{OC}=22.1V, I_{SC}=8.37A, V_{MP}=17.7V, I_{MP}=7.63A, P_{MAX}=135W, FF=0.733). Simulation and experiment test conditions and components values are shown in Table II. The results are for specified test conditions, (1 to I_{MAX} A current input, δ=0.3 to 0.9 duty cycle, and G=200 to 1000 W/m² radiation). Three dimension plots of overall efficiency, PV efficiency, dc-to-dc converter efficiency, and input ripple current versus both the input current and the duty cycle, are shown in Fig. 10. The same efficiencies and input ripple current versus both the input current and the irradiation are shown in Fig. 11.

Fig. 10d presents the input current ripple for the three converters, the Ćuk, C and D converters for different irradiation levels; from 200W/m² to 1000W/m². The D converter characteristics are in green, while the Ćuk and C converter result are in black and red respectively. The MPP current at 200W/m² for the module is 1.453A, while the MPP current for irradiation levels 600, and 1000W/m² are 4.55A, and 7.68A respectively. Also, intermediate readings between 1A and the MPP current cover the area affected by input current ripple. In Fig. 10d, the input current ripple of the D converter is low compare to that of the Ćuk and C converters. Fig. 10c shows the efficiency of the dc-to-dc converter excluding the ripple effect and the efficiency of the PV module (which is the average power of the dc-to-dc converter input divided by the corresponding maximum power of the PV module). Fig. 10b clarifies the PV efficiency while Fig. 10a presents the combination of Fig. 10c (dc-to-dc converter efficiency) and Fig. 10b (PV efficiency), giving the overall efficiency of the dc-to-dc converter system. Clearly, the relation between Fig. 10d and Fig. 10c is an inversely proportional relationship; when the input current ripple is low, the PV efficiency is high.

To show the effect of the input current ripple at constant duty cycle by varying the irradiance level, Fig. 11d shows the input current ripple for the three converters for different duty cycle values; from 0.3 to 0.9. Fig. 11c shows the efficiency of the dc-to-dc converter excluding the PV efficiency, while Fig. 11b clarifies the PV efficiency and Fig. 11a presents overall efficiency of the dc-to-dc converter system. Similarly, Fig. 11d is inversely proportional with Fig. 11b, while Fig. 11c depends on the dc-to-dc converter itself and Fig. 11a is the combination of both efficiencies.

Normally, the steady-state error and the lack of output regulation are expected for the simulation results when compared to the theoretical calculations since they are based on an ideal switch and diode and lossless capacitors and inductors.

The PV efficiency is the transferred efficiency from the PV to the terminals of the dc-to-dc converter. The dc-to-dc converter efficiency is the power transfer ratio, excluding some converter losses; for example copper losses. The overall system efficiency is the combination of the PV and the dc-to-dc converter efficiencies, which is the ratio of the converter output power to the PV input power.

The three topologies have near identical waveforms, other than the inductor input or output ripple currents. The D converter has the lowest input ripple current because the input inductor only experiences the capacitor voltage ripple. This low-ripple topology property has not been previously recognized, hence has not been exploited for PV or fuel cell interfacing. A low-ripple current consequence is that the common inductor conducts both the input and output currents, hence has higher I^2R losses. These losses are noted to be proportionally smaller for low current, hence result in small differences between the dc-to-dc efficiencies for the three converters. The challenge here, as shown in Fig. 11, is that with low input current and low irradiation, the PV efficiency becomes significantly higher for the D converter compared to the $Ćuk$ and C converters. Therefore, the overall efficiency is higher for the D converter at lower current and irradiation. Although the $Ćuk$ converter has a higher dc-to-dc converter efficiency, especially for high current, the D converter yields higher overall system efficiency due to the higher PV efficiency.

TABLE II
DC-TO-DC CONVERTER COMPONENTS

E	V_{OC}=22.1V, I_{SC}=8.37A, V_{MP}=17.7V, I_{MP}=7.63A, P_{MAX}=135W, FF=0.733		T, mosfet	200V, 0.54mΩ
L_1	1.0mH, 74mΩ, 10.6A		D, SiC	600V, 10A
L_2	1.0mH, 74mΩ, 10.6A		$δ$	30−90%
C	10µF, 250V		f	50kHz
G	200−1000W/m²		I_i	1−7.68A

Referring to Fig. 10, PV efficiency is minimally affected by changing the duty cycle. But dc-to-dc converter efficiency is affected by changing the duty cycle; efficiency decreases on the boundaries - like 0.3 and 0.9 duty cycles. Fig. 10 presents the efficiency for the PV curve knee at the MPP for each selected irradiation (1.453A, 4.55A, and 7.68A). For MPP current, the low ripple current effect on D converter clearly manifests in the overall efficiency. Similarly, by decreasing the input current and the duty cycle in the mid-range, the D converter overall efficiency increases. The $Ćuk$ converter overall efficiency increases for high current, unlike the MPP current, where the effect of the ripple current increases, as described in section II.

Fig. 13 shows practical time domain transient waveforms for the three considered converters. The practical data measures the overall efficiency and the input ripple current. Fig. 13 shows a specific example for 800W/m² at 0.5 duty cycle and 2A.

The experiment results in Fig. 15 verify the simulations for the three converter systems. The practical results in this figure present the overall efficiency and the input current ripple at different irradiations (600W/m², 800W/m² and 1000W/m²), hence at different input currents, varied from 1A to the MPP current. For the MPP current, the effect of the low ripple current on D converter clearly manifested on the overall efficiency. Similarly, by decreasing the input current and the duty cycle in the mid-range, the overall efficiency of the D converter system increases. The overall efficiency of the $Ćuk$ converter system increases for high current, unlike the current at the MPP, where the effect of the ripple current increases.

Converters without inductance in both the input and output have the highest copper losses; hence the lowest dc-to-dc efficiency, but not necessarily the lowest overall system efficiency because the PV efficiency factor is independent of copper losses. Similarly, converters with high input ripple current ($Ćuk$ and C) have the highest ripple-power losses; hence lowest PV efficiency. Thus the converter with lowest input ripple (D converter) has the highest PV efficiency; which offsets the penalty of lower dc-to-dc converter efficiency; therefore, result in the highest overall system efficiency. The experiment results show that the efficiency of the D converter increases when the current decreases at high irradiation, while for low irradiation the efficiency increases. The difference between the efficiencies for the D and $Ćuk$ converters increases by decreasing the irradiation and input current.

VI. CONCLUSION

This paper considered three buck-boost converters that avoid the need to electrolytically capacitor filter PV arrays from the dc-to-dc converter input. The buck-boost D converter, that offers continuous low ripple input current is suitable for photovoltaic module MPP tracking, has been proposed. The D converter has been compared to two other converters with the same transfer function, same number of components, but different topologies. Analysis of the D converter established the transfer function and the input ripple current and proved that the D converter has the lowest input ripple current of the three converters. The efficiency degrading effect of the input ripple current on the photovoltaic module has been established. Simulations showed which of the three topologies offered the lowest input ripple current and the highest efficiency. Practical results authenticated the simulations. The D converter offers the lowest input ripple current, since the input inductor experiences only modest impressed voltages. The $Ćuk$ and C converters have the same input ripple current magnitude with the C converter having a lower efficiency than the $Ćuk$ converter. When accounting for photovoltaic interfacing, the D converter input-ripple current results in higher PV efficiency that offsets the drawback of lower converter efficiency. By increasing the input inductance, the $Ćuk$ converter input ripple current decreases resulting in increased PV efficiency but the cost of higher inductance increases too.
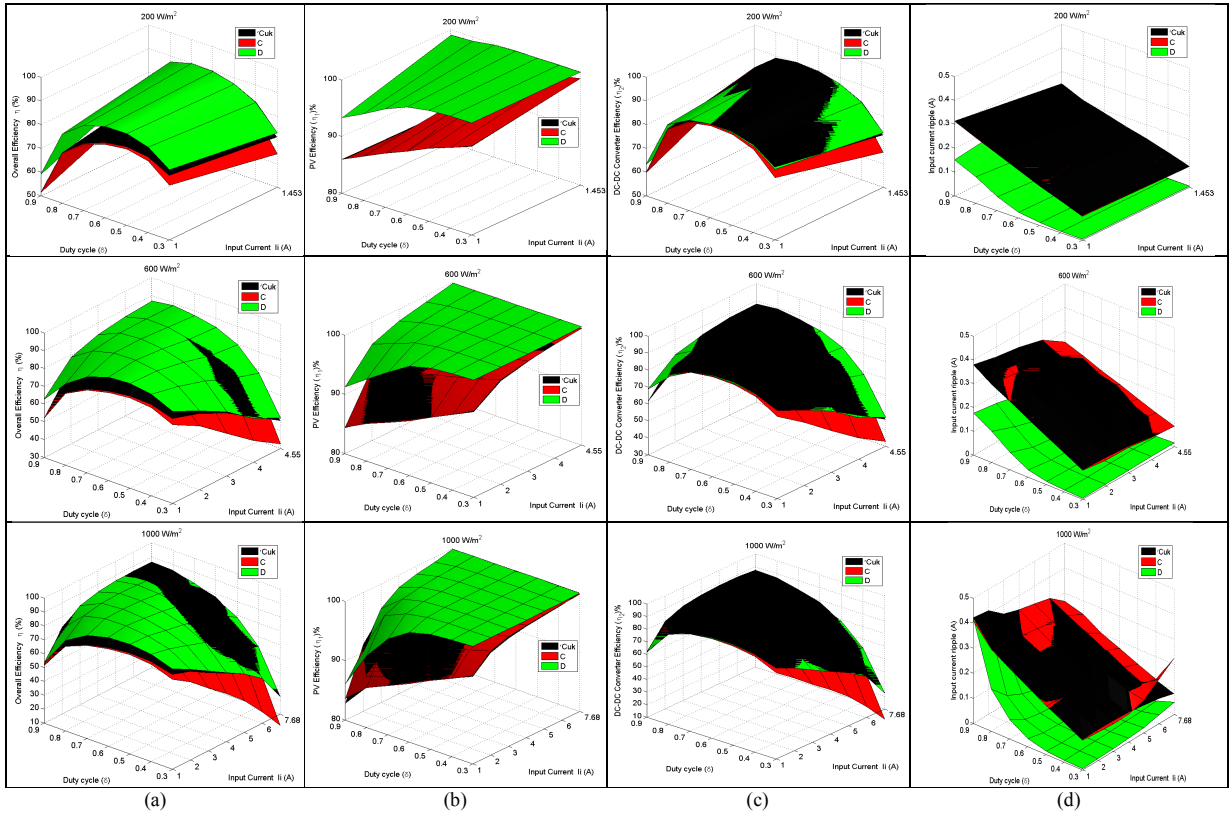
Fig. 10: Simulation of the input current (including MPP current) versus duty cycle for (a) overall efficiency, (b) PV efficiency, (c) dc-to-dc converter efficiency, and (d) input ripple current.
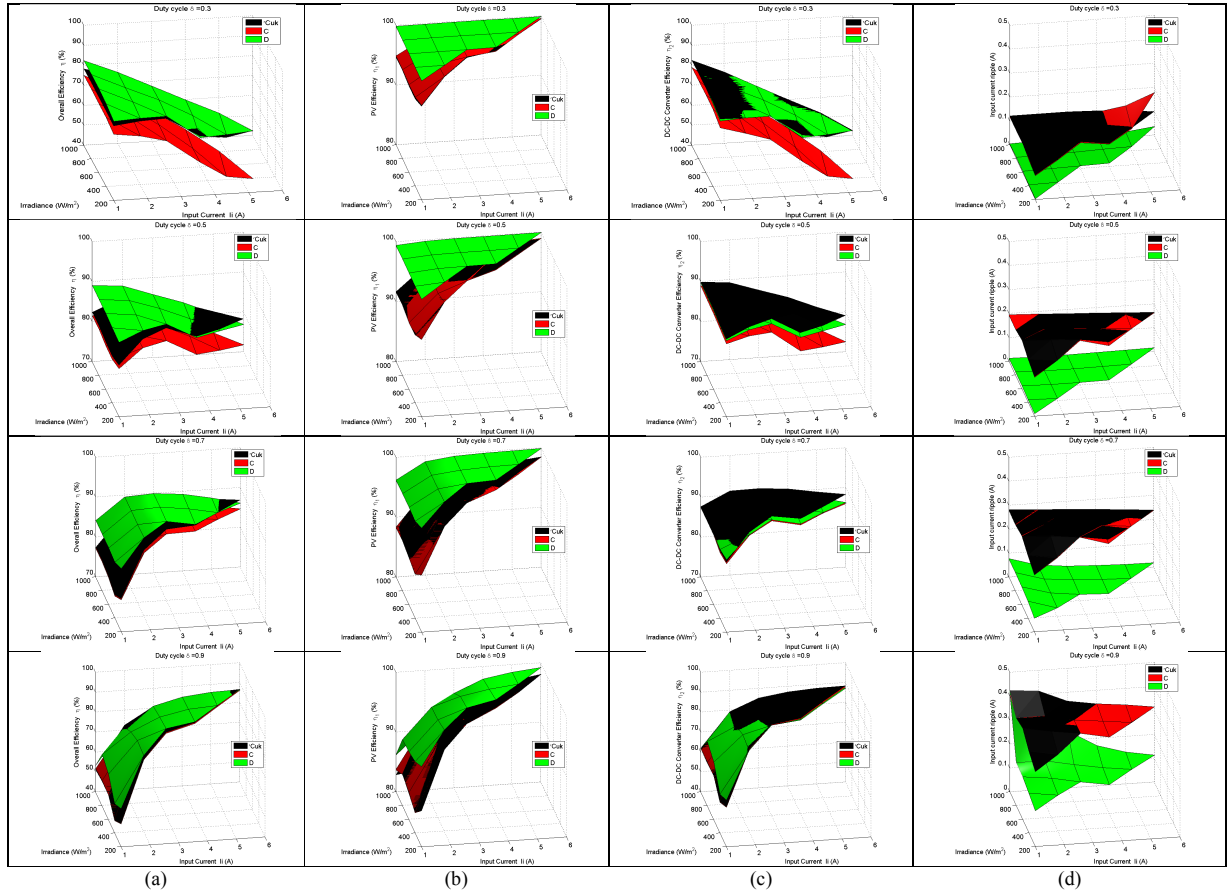

Fig. 11: Simulation of the input current versus irradiation for (a) overall efficiency, (b) PV efficiency, (c) dc-to-dc converter efficiency, and (d) input ripple current.
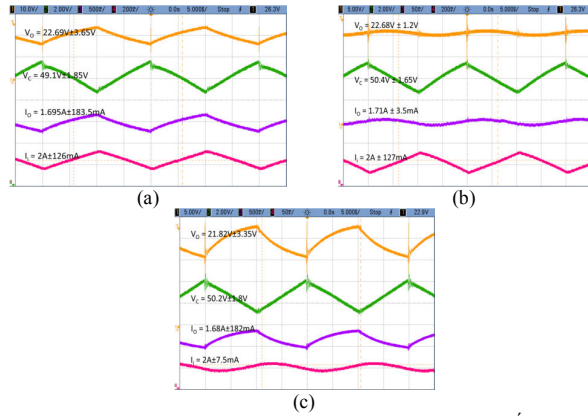
(a)   (b)

(c)

Fig. 13: Time domain transient practical waveforms for the (a) Ćuk, (b) C, and (c) D converters.
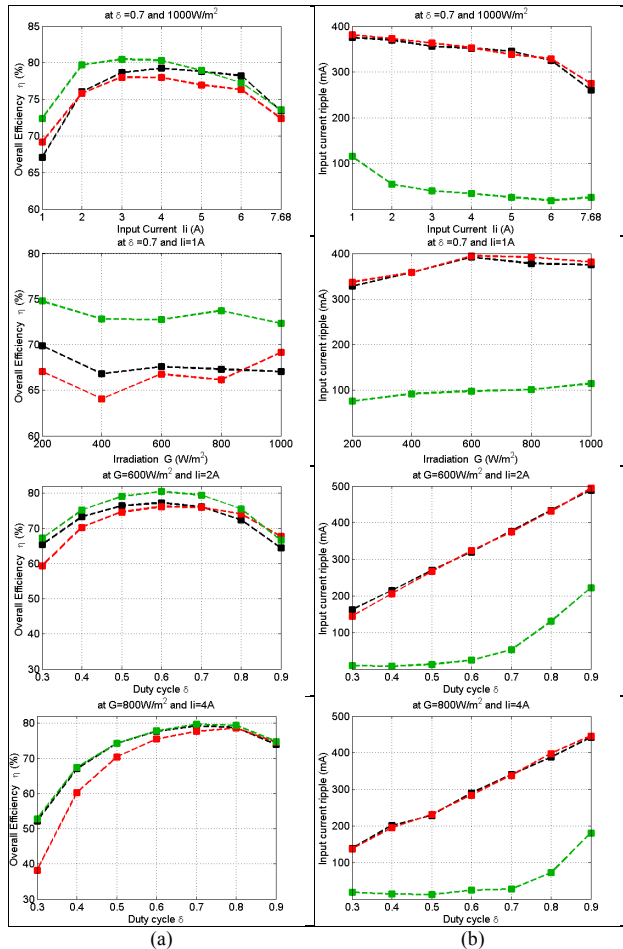

(a)   (b)

Fig. 15: Practical results for (a) overall efficiency and (b) input ripple current

REFERENCES

[1] Kondrath, N.; Kazimierczuk, M.K.; "Loop gain and margins of stability of inner-current loop of peak current-mode-controlled PWM dc-dc converters in continuous conduction mode," Power Electronics, IET, vol.4, no.6, pp.701-707, July 2011

[2] Yi-Ping Hsieh; Jiann-Fuh Chen; Tsorng-Juu Liang; Lung-Sheng Yang, "Novel High Step-Up DC–DC Converter for Distributed Generation System," Industrial Electronics, IEEE Transactions on , vol.60, no.4, pp.1473,1482, April 2013

[3] Williams, B., "GENERATION AND ANALYSIS OF CANONICAL SWITCHING CELL DC-TO-DC CONVERTERS," Industrial Electronics, IEEE Transactions on , vol.PP, no.99, pp.1,1, 0

[4] Williams, B.W.; "DC-to-DC Converters with Continuous Input and Output Power," Power Electronics, IEEE Transactions on, vol.28, no.5, pp.2307-2316, May 2013

[5] Hongbo Ma; Jih-Sheng Lai; Quanyuan Feng; Wensong Yu; Cong Zheng; Zheng Zhao, "A Novel Valley-Fill SEPIC-Derived Power Supply Without Electrolytic Capacitor for LED Lighting Application," Power Electronics, IEEE Transactions on , vol.27, no.6, pp.3057,3071, June 2012

[6] Shu Wang; Xinbo Ruan; Kai Yao; Siew-Chong Tan; Yang Yang; Zhihong Ye, "A Flicker-Free Electrolytic Capacitor-Less AC–DC LED Driver," Power Electronics, IEEE Transactions on , vol.27, no.11, pp.4540,4548, Nov. 2012

[7] Chung, H.S.-H.; Ngai-Man Ho; Wei Yan; Tam, P.W.; Hui, S.Y., "Comparison of Dimmable Electromagnetic and Electronic Ballast Systems-An Assessment on Energy Efficiency and Lifetime," Industrial Electronics, IEEE Transactions on , vol.54, no.6, pp.3145,3154, Dec. 2007

[8] Hui, S.S.Y.R.; Si Nan Li; Xue Hui Tao; Wu Chen; Ng, W. M., "A Novel Passive Offline LED Driver With Long Lifetime," Power Electronics, IEEE Transactions on , vol.25, no.10, pp.2665,2672, Oct. 2010

[9] Jenkins, D. P.; Fletcher, J.; Kane, D., "Lifetime prediction and sizing of lead-acid batteries for microgeneration storage applications," Renewable Power Generation, IET , vol.2, no.3, pp.191,200, September 2008

[10] Kjaer, S.B.; Pedersen, J.K.; Blaabjerg, F.; "A review of single-phase grid-connected inverters for photovoltaic modules," Industry Applications, IEEE Transactions on, vol.41, no.5, pp. 1292- 1306, Sept.-Oct. 2005

[11] Yaosuo Xue; Liuchen Chang; Sren Baekhj Kjaer; Bordonau, J.; Shimizu, T.; "Topologies of single-phase inverters for small distributed power generators: an overview," Power Electronics, IEEE Transactions on, vol.19, no.5, pp. 1305- 1314, Sept. 2004

[12] Quan Li; Wolfs, P.; "A Review of the Single Phase Photovoltaic Module Integrated Converter Topologies With Three Different DC Link Configurations," Power Electronics, IEEE Transactions on, vol.23, no.3, pp.1320-1333, May 2008

[13] Myrzik, J.M.A.; Calais, M.; "String and module integrated inverters for single-phase grid connected photovoltaic systems - a review," Power Tech Conference Proceedings, 2003 IEEE Bologna , vol.2, no., pp. 8 pp. Vol.2, 23-26 June 2003

[14] Selvaraj, J.; Rahim, N.A.; "Multilevel Inverter For Grid-Connected PV System Employing Digital PI Controller," Industrial Electronics, IEEE Transactions on, vol.56, no.1, pp.149-158, Jan. 2009

[15] Sullivan, C.R.; Awerbuch, J.J.; Latham, A.M., "Decrease in Photovoltaic Power Output from Ripple: Simple General Calculation and the Effect of Partial Shading," Power Electronics, IEEE Transactions on, vol.28, no.2, pp.740,747, Feb. 2013

[16] S. B. Kjær, "Design and control of an inverter for photovoltaic applications," Ph.D. dissertation, Dept. Energy Technol., Inst. Energy Technol., Aalborg University, Aalborg, Denmark, 2005.

[17] Benavides, N.D.; Chapman, P.L., "Modeling the Effect of Voltage Ripple on the Power Output of Photovoltaic Modules," Industrial Electronics, IEEE Transactions on, vol.55, no.7, pp.2638,2643, July 2008

[18] Sullivan, C.R.; Awerbuch, J.; Latham, A.M., "Decrease in photovoltaic power output from ripple: Simple general calculation and effect of partial shading," Applied Power Electronics Conference and Exposition (APEC), 2011 Twenty-Sixth Annual IEEE , vol., no., pp.1954,1960, 6-11 March 2011

[19] Zengshi Chen; "PI and Sliding Mode Control of a Ćuk Converter, " Power Electronics, IEEE Transactions on, vol.27, no.8, pp.3695-3703, Aug. 2012

[20] Mishima, T.; Nakaoka, M., "A Practical ZCS-PWM Boost DC-DC Converter With Clamping Diode-Assisted Active Edge-Resonant Cell and Its Extended Topologies," Industrial Electronics, IEEE Transactions on , vol.60, no.6, pp.2225,2236, June 2013

[21] Ming Qin; Jianping Xu, "Improved Pulse Regulation Control Technique for Switching DC–DC Converters Operating in DCM," Industrial Electronics, IEEE Transactions on , vol.60, no.5, pp.1819,1830, May 2013

[22] Babaei, E.; Seyed Mahmoodieh, M.E.; Mashinchi Mahery, H., "Operational Modes and Output-Voltage-Ripple Analysis and Design Considerations of Buck–Boost DC–DC Converters," Industrial Electronics, IEEE Transactions on, vol.59, no.1, pp.381,391, Jan. 2012

[23] Hyun-Lark Do; "Improved ZVS DC-DC Converter with a High Voltage Gain and a Ripple-Free Input Current," Circuits and Systems I: Regular Papers, IEEE Transactions on, vol.59, no.4, pp.846-853, April 2012

[24] Jong-Jae Lee; Bong-Hwan Kwon; "Active-Clamped Ripple-Free DC/DC Converter Using an Input–Output Coupled Inductor," Industrial Electronics, IEEE Transactions on, vol.55, no.4, pp.1842-1854, April 2008